

基于波长到时间映射快速测量纠缠光子 相位匹配波长的实验方法

李百宏^{1,2}, 夏志广^{1,2}, 项晓^{2,3*}, 靳亚晴^{2,3}, 权润爱^{2,3}, 董瑞芳^{2,3**}, 刘涛^{2,3}, 张首刚^{2,3}

¹ 西安科技大学理学院, 陕西 西安 710054;

² 中国科学院国家授时中心中国科学院时间频率基准重点实验室, 陕西 西安 710600;

³ 中国科学院大学天文与空间科学学院, 北京 100049

摘要 准相位匹配有利于实现高效的自发参量下转换, 它由非线性晶体的极化周期和依赖于温度的折射率决定。为了确定特定波长处所需的晶体温度, 需要测量相位匹配波长随晶体温度的变化关系。单色仪的传统测量方法具有测量精度较低且耗时长等缺点。提出了一种实验方法, 该方法能快速准确测量纠缠光子相位匹配波长随晶体温度变化的关系。在信号和闲置光路中先后加入色散元件, 通过测量纠缠光子对到达时间关联峰值处的时间延迟随晶体温度的变化关系, 利用波长到时间的映射关系将其转化为波长随晶体温度的变化关系。给出了周期极化铌酸锂(PPLN)波导和周期极化磷酸氧钛钾(PPKTP)晶体的实验测量结果, 测量精度优于 0.1 nm, 测量时间约为几分钟。测量精度受限于单光子探测器的抖动时间和色散元件色散量的大小。原则上, 抖动时间越小, 色散量越大, 测量精度越高。最后讨论了 Sellmeier 方程计算的结果与实验结果存在差异的可能原因。所提方法可以用来校准相位匹配波长与晶体温度的关系及极化周期, 并有望实现温度依赖的 Sellmeier 方程的修正或改进。

关键词 量子光学; 纠缠光子; 相位匹配波长; 晶体温度; 波长到时间映射

中图分类号 O431.2

文献标志码 A

doi: 10.3788/CJL202148.0312001

1 引言

自发参量下转换(SPDC)过程产生的纠缠源在量子精密测量^[1-4]、量子光谱^[5-11]、量子成像^[12-15]、量子隐形传态^[16-18]和量子安全通讯^[19-21]等领域中具有广泛的应用价值。但只有满足相位匹配条件(动量守恒)时才能实现高效的 SPDC。自然条件下只有部分双折射晶体能满足相位匹配条件, 这限制了纠缠光子的相位匹配波长和带宽。因此, 准相位匹配技术^[22-23]应运而生, 它是通过对非线性晶体的不同部分施加周期性电极来调制晶体的极化率, 进而实现准相位匹配。准相位匹配由晶体的极化周期和

晶体的折射率决定。而折射率可以通过晶体温度来调节, 不同的晶体温度对应着不同的相位匹配波长。为了确定所需要的相位匹配波长处的晶体温度, 就需要确定相位匹配波长随晶体温度的变化关系。这种关系可以通过温度依赖的 Sellmeier 方程来估算^[24-27]。对于 SPDC 过程产生的纠缠光源, 根据温度依赖的 Sellmeier 方程可知, 通过调节非线性晶体的温度可以调节群速度匹配波长和相位匹配波长, 从而精确地操控量子态的光谱分布及其波长范围^[24]。不同的量子态有着不同的应用价值, 因此研究 SPDC 过程中晶体温度对量子态的操控是非常必要和重要的, 晶体温度也已成为实验中常用的一种

收稿日期: 2020-08-17; 修回日期: 2020-09-01; 录用日期: 2020-09-22

基金项目: 国家自然科学基金(12074309, 12033007, 61801458, 61875205, 91836301)、中国科学院前沿科学重点研究计划(QYZDB-SSW-SLH007)、中国科学院战略性先导科技 C 类专项(XDC07020200)、中国科学院重点部署项目(ZDRW-KT-2019-1-0103)、广东省重点领域研发计划(2018B030325001)、中国科学院“西部之光”B 类计划(XAB2019B17, XAB2019B15)、陕西省自然科学基金基础研究计划项目(2019JM-346)、西安科技大学优秀青年基金(2019YQ2-13)

* E-mail: xiangxiao@ntsc.ac.cn; ** E-mail: dongruifang@ntsc.ac.cn

精确操控量子态的重要手段^[28-30]。然而,很多非线性晶体的 Sellmeier 方程仍然是未知的。即使 Sellmeier 方程已知,由于 Sellmeier 方程中的系数来自于经验值,估算的结果和实验的结果在一些特殊的波长和温度范围下仍然存在着差异^[27],需要不断地对 Sellmeier 方程进行修正^[31]或改进^[32]。因此,利用实验方法快速准确测量 SPDC 过程中的纠缠光子相位匹配波长就显得十分必要。在实验上,通常利用单色仪来测量纠缠光子光谱及相位匹配波长随晶体温度的变化关系^[28-29,33]。2012 年,日本的 Kakuno 等^[30]在 MgO-Doped LiNbO₃ 波导中,利用传统的光谱仪测量了相位匹配波长随晶体温度的变化关系,并在不同波导温度下获得了简并和非简并的纠缠光子对。2018 年,张越等^[33]利用单色仪测量了由 II 类周期极化铌酸锂波导产生的纠缠光子光谱,从而得到了相位匹配波长随波导温度的变化关系。然而,单色仪和传统光谱仪需要在不同晶体温度下扫描不同的波长,因此测量精度较低且很耗时^[33],特别是对于宽带的纠缠光谱。

本文提出了一种可以快速测量纠缠光子相位匹配波长随晶体温度变化的实验方法。该方法利用了波长到时间的映射技术^[11, 34-36],通过加入色散元件,将波长测量转换为纠缠光子到达时间关联的测量。在信号光和闲置光路径中,通过先后加入色散元件,测量不同晶体温度下两光子对到达时间的延迟,利用波长到时间的映射将时间延迟随晶体温度的变化关系转化为信号光和闲置光波长随晶体温度的变化关系。利用此方法对周期极化铌酸锂(PPLN)波导和周期极化磷酸氧钛钾(PPKTP)晶体进行了测量。最后分析了测量精度的影响因素及 Sellmeier 方程计算的结果与实验结果的差异,并讨论了本文方法的优缺点及其他可能的一些应用。

2 原理和方法

为了实现高效的 SPDC 过程,需要同时满足以下两个条件:

$$\frac{1}{\lambda_p} - \frac{1}{\lambda_s} - \frac{1}{\lambda_i} = 0, \quad (1)$$

$$\Delta k = 2\pi[n_p(T)/\lambda_p - n_s(T)/\lambda_s - n_i(T)/\lambda_i \pm 2\pi/\Lambda] = 0, \quad (2)$$

式中:p,s,i 分别代表泵浦光,信号光和闲置光; n 为折射率; λ 为波长; Λ 为非线性晶体的极化周期; T 为温度。(1)式和(2)式分别代表能量守恒定律和动量守恒定律。(2)式也被称为准相位匹配条件,

对应的波长称为相位匹配波长。由于折射率是晶体温度 T 的函数,因此通过改变晶体温度可以操控相位匹配波长。

在纠缠光子对进入探测器探测之前,在信号光(或闲置光)路径中插入色散元件,当色散量满足远场条件时,信号光和闲置光到达时间的关系可以表示为二阶 Glauber 关联函数^[11]:

$$G^{(2)}(\tau) \propto \exp\left[-\frac{(\tau - \bar{\tau})^2}{2\Delta}\right], \quad (3)$$

式中: τ 为信号光和闲置光之间的延迟时间; Δ 为关联函数的宽度,在没有滤波的情况下,它由色散元件的色散量和纠缠光子的带宽决定; $\bar{\tau}$ 为纠缠光子在关联函数中心位置处的延迟时间^[11],具体表示为

$$\bar{\tau} = \tau_0 + \beta l \tilde{\omega}, \quad (4)$$

式中: $\tau_0 = (\tau_{D1} + \tau_1) - (\tau_{D2} + \tau_2)$,其中 τ_{D1}, τ_{D2} 分别为探测器 D1 和 D2 的抖动时间, τ_1, τ_2 分别为信号光和闲置光的路径延时; β 为色散元件的群速度色散,单位为 ps²/m; l 为色散元件(如光纤)的长度; βl 即为色散元件引入的总色散量。在中心角频率为 $2\omega_0$ 的连续激光泵浦的 SPDC 过程中,纠缠光子对是频率反关联的,即 $\omega_s = \omega_{s,0} + \tilde{\omega}, \omega_i = \omega_{i,0} - \tilde{\omega}$,其中 ω_s 和 ω_i 分别为信号光和闲置光的角频率, $\omega_{s,0}$ 和 $\omega_{i,0}$ 分别为信号光和闲置光的中心角频率, $\tilde{\omega}$ 为信号光角频率相对于中心角频率的失谐量。将色散元件分别插入信号光和闲置光路径时,对应的时间延迟 $\bar{\tau}_s, \bar{\tau}_i$ 分别为

$$\bar{\tau}_s = \tau_0 + \beta l \tilde{\omega}, \quad (5)$$

$$\bar{\tau}_i = \tau_0 - \beta l \tilde{\omega}. \quad (6)$$

为了方便起见,用波长代替角频率,此时 $\bar{\tau}_{s,i} = \tau_0 \pm D l \lambda_{s,i}$,其中 $D = -2\pi c \beta / \lambda_{s,i}^2$ 为群速度色散参数,单位为 ps/(nm·km)。根据(5)、(6)式可知,在实验中可以通过调节非线性晶体的温度来获得信号光和闲置光的时间延迟随晶体温度的变化关系。利用波长到时间的映射关系,可以将时间延迟随晶体温度的变化关系转化为波长随晶体温度的变化关系。若信号光和闲置光路径间的时间延迟相等,即 $\bar{\tau}_s = \bar{\tau}_i$,则 $\tilde{\omega} = 0, \omega_{s,0} = \omega_{i,0} = \omega_0$,此时两光子的频率(波长)是简并的。两曲线交叉点处的温度 T_D 即为对应的波长简并点的晶体温度,其余为非简并波长点的晶体温度。

随着超导纳米线单光子探测器的发展,其探测效率可达 90% 以上,抖动时间低于几十皮秒^[37],因此具有高精度的时间分辨率。利用色散元件,使不

同波长的纠缠光子在不同时间内到达探测器,将高精度的时间分辨率转化为高精度的光谱分辨率 ($<0.1 \text{ nm}$)。而纠缠光子的到达时间是可以快速获取和处理的,因此所提方法的测量时间很短,约为几分钟。

3 实验装置及实验结果

3.1 实验装置

实验装置如图 1 所示,其中 FBG 为光纤布拉格光栅,FC 为光纤耦合器,FPBS 为光纤偏振分束器,HWP 为半波片,LPs 为长通滤波,SNSPD 为超导纳米线单光子探测器,TCSPC 为时间关联单光子计数模块。利用波长为 780 nm 的连续分布式布拉格反射激光器泵浦长度为 10 mm 的第 II 类 PPLN 波导(极化周期约为 $8.4 \mu\text{m}$),通过 SPDC 过程产生频率反关联(能量-时间)纠缠源。半波片 HWP1 用来调节泵浦激光的偏振态,从而优化 SPDC 产生效率。利用两个长通滤波器滤掉残余的泵浦光后,信号和闲置光子被聚焦耦合进光纤偏振分数器中。半波片 HWP2 将信号和闲置光子分开,使其进入两个互相正交的偏振光纤路径中。

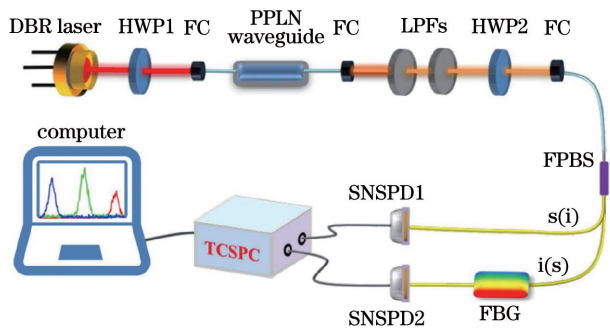


图 1 实验装置

Fig. 1 Experimental setup

实验中用到的色散元件为光纤布拉格光栅,将其放置在信号光或闲置光路径上以实现基于色散的波长到时间的映射转换。利用两个超导纳米线单光子探测器(探测效率为 50% , 时间抖动约为 56 ps)探测光子的到达时间。利用时间关联单光子计数模块(TCSPC)测量两光子的二阶 Glauber 关联分布。

为了能够准确得到波长和时间的映射关系,实验前先要完成波长与时间延迟关系的测量,从而校准波长到时间的映射关系^[11]。通过实验得到纠缠光子波长和时间延迟的线性关系为 $\bar{\tau} = 893203 - 523.6\lambda$ 。利用此关系,可以估计 FBG 在 1560 nm 处有 $Dl = -(523.6 \pm 2.2) (\text{ps}/\text{nm})$ 。

3.2 实验结果

利用 10 mm 长的第 II 类 PPLN 波导测量得到的时间延迟随波导温度的变化关系如图 2(a) 所示。方点和圆点分别代表 FBG 插入 s 和 i 路径的实验结果。可以看到,两曲线有个交叉点,此交叉点的时间延迟相等,对应的温度即为波长简并点的波导温度 ($T_D = 45.1 \text{ }^\circ\text{C}$),其他位置为非简并点的波导温度。为了准确确定简并波长处的波导温度 T_D ,在 T_D 附近采集较多数据。实验中 PPLN 波导的温控精度为 $0.1 \text{ }^\circ\text{C}$ 。利用波长到时间的映射关系,将图 2(a) 中时间延迟随波导温度的变化关系转换成波长随温度的变化关系,如图 2(b) 所示。图 2(b) 给出了不同波导温度下信号光和闲置光的中心波长随波导温度的变化关系,两直线的交点即为波长简并点,简并波长为 1560.1 nm 。图 2 中的实线为线性拟合结果,可以看到,线性拟合结果和实验结果吻合很好。误差棒代表多次测量得到的标准偏差。

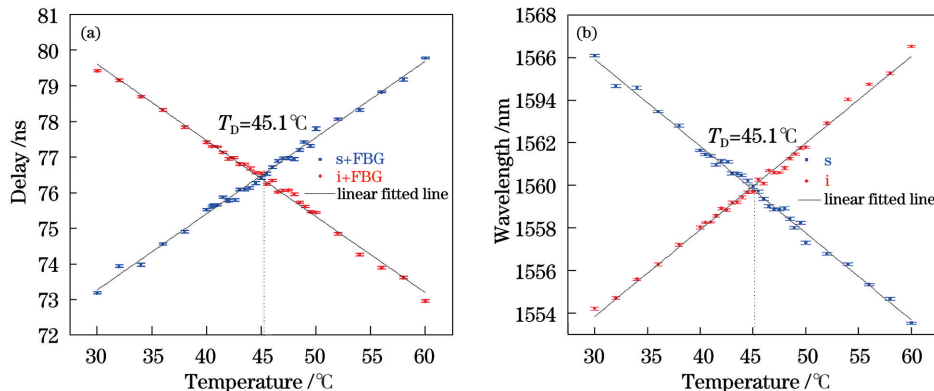


图 2 测量结果。(a) 时间延迟随 PPLN 波导温度的变化;(b) 基于波长到时间的映射关系重建的波长随温度的变化

Fig. 2 Measurement results. (a) Time delay versus temperature of PPLN waveguide; (b) reconstructed wavelength versus temperature based on wavelength-to-time mapping

为了说明所提方法的普遍适用性,对 10 mm 长的第 II 类 PPKTP 晶体(极化周期为 $46.146 \mu\text{m}$)也进行了实验测试。在实验中,采用基于 InGaAs 雪崩光电二极管的近红外单光子探测器进行光子探测。探测前同样进行了波长到时间映射关系的校准。通过实验,得到纠缠光子波长和时间延迟的线

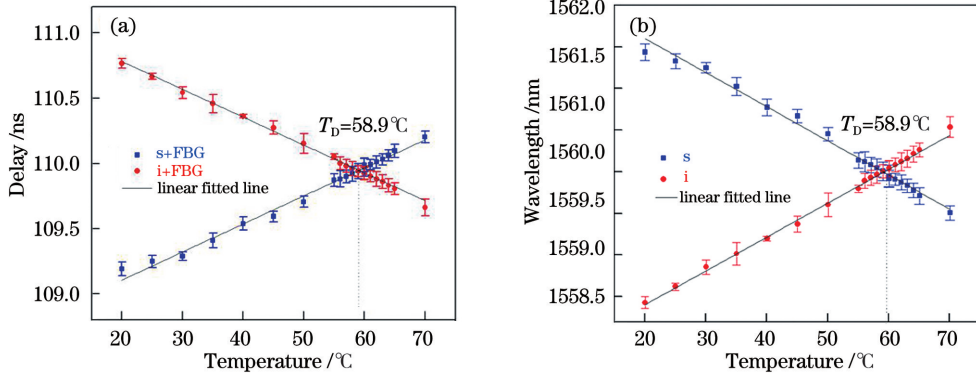


图 3 测量结果。(a)时间延迟随 PPKTP 晶体温度的变化;(b)基于波长到时间的映射关系重建的波长随温度的变化
Fig. 3 Measurement results. (a) Time delay versus temperature of PPKTP crystal; (b) reconstructed wavelength versus temperature based on wavelength-to-time mapping

4 分析与讨论

通过精准控制晶体或波导温度,可以精确地操控纠缠光子的光谱分布,这是实验中经常用到的一种重要的操控手段。利用基于色散的波长到时间映射技术,可以快速测量纠缠光子波长随晶体温度的变化。因此,利用本文所提方法可以快速测量非线性晶体特别是一些 Sellmeier 方程未知的非线性晶体或波导产生的纠缠光子的波长随晶体温度的变化关系,从而为各种应用中的纠缠源选择提供参考。测量图 2(a)中的所有数据花了几分钟时间,比起单色仪方法^[33]的测量时间(几小时)大大减小。此方法的测量精度主要受限于探测器的时间抖动和所加色散元件色散量的大小。图 2(a)的标准偏差的最大值为 47 ps,标准偏差的均值为 32 ps,利用波长与时间的映射关系,可以得到波长的测量精度约为 0.09 nm,因此图 2(b)的波长测量精度优于 0.1 nm。图 3(a)的标准偏差的最大值为 143 ps,标准偏差的均值为 92 ps,利用波长与时间的映射关系,可以得到波长的测量精度约为 0.27 nm,因此图 3(b)的波长测量精度优于 0.27 nm。两者的差别在于前者用抖动时间较小(半峰全宽约为 56 ps)的超导纳米线单光子探测器探测光子,而后者用抖动时间较大(半峰全宽约为 200 ps)的半导体探测器探测光子。原则上,探测器的抖动时间越小,色散元件的

性关系为 $\bar{\tau} = 926759 - 523.6\lambda$ 。实验结果如图 3 所示,获得的波长简并点的晶体温度 T_D 为 $58.9 \text{ }^\circ\text{C}$,简并波长为 1560.0 nm 。从以上结果可以看到,晶体温度会影响纠缠光子对的波长简并性,从而影响纠缠光子对的光谱不可分性^[38]和 Hong-Ou-Mandel 干涉可见度^[39]。

色散量越大,测量精度越高。

此外,通过理论计算可知,在一定的晶体温度范围内,相位匹配波长随晶体温度的变化是线性的,这一点在图 2 和图 3 中得到印证。另外,基于 PPLN 波导和 PPKTP 晶体的 Sellmeier 方程^[26-27]及相位匹配条件,计算得到了相位匹配波长随温度的变化关系,结果显示,只有当极化周期为 $9.263 \mu\text{m}$ 和 $46.027 \mu\text{m}$ 时,才能得到与实验结果相同的简并点温度。而 PPLN 波导和 PPKTP 晶体标注的极化周期分别为 $8.4 \mu\text{m}$ 和 $46.146 \mu\text{m}$ 。由于制作工艺水平的限制,所生产的极化周期与设计值存在一定的偏差,这将对相位匹配波长与晶体温度的关系产生影响。因此,利用实验方法准确快速地确定纠缠光子波长随晶体温度的变化关系就显得尤为重要。反过来,将所提方法测量到的纠缠光子相位波长随晶体温度的变化关系与 Sellmeier 方程得到的结果进行对比,进而校准相位匹配波长与晶体温度的关系及极化周期,并有望实现对 Sellmeier 方程的修正或改进。比较图 2 和图 3 还可以看到,两种晶体对温度的敏感性是不同的,相比之下,PPLN 波导对温度的变化更加敏感。这种特性决定了它们有不同的用途,如温度敏感的非线性晶体可应用于量子遥感领域^[40]。

总之,所提方法不仅能快速准确地测量纠缠光子相位匹配波长随晶体温度的变化关系,还能实现

信号光和闲置光的单光子频谱及联合频谱的快速测量^[11]。实验中所用的色散元件还可以替换为单模光纤或色散补偿光纤等,只要色散量足够大且满足远场条件即可。

5 结 论

提出了一种基于波长到时间映射技术的实验方法,该方法能快速准确测量纠缠光子相位匹配波长随晶体温度变化的关系。无需使用单色仪和光谱仪,通过测量纠缠光子到达时间关联峰值处对应的时间延迟随晶体温度的变化,利用波长到时间的映射关系,快速准确确定相位匹配波长。与传统方法相比,此方法的测量时间仅需几分钟。给出了 PPLN 波导和 PPKTP 晶体的测量结果,测量精度优于 0.1 nm。测量精度受限于单光子探测器的抖动时间和色散元件的色散大小。此方法可以用来校准相位匹配波长与晶体温度的关系及极化周期,并有望实现温度依赖的 Sellmeier 方程的修正或改进。

参 考 文 献

- [1] Giovannetti V, Lloyd S, Maccone L. Quantum-enhanced positioning and clock synchronization [J]. *Nature*, 2001, 412(6845): 417-419.
- [2] Nasr M B, Minaeva O, Goltsman G N, et al. Submicron axial resolution in an ultrabroadband two-photon interferometer using superconducting single-photon detectors [J]. *Optics Express*, 2008, 16(19): 15104-15108.
- [3] Quan R, Dong R, Zhai Y, et al. Simulation and realization of a second-order quantum-interference-based quantum clock synchronization at the femtosecond level [J]. *Optics Letters*, 2019, 44(3): 614-617.
- [4] Hou F Y, Quan R N, Dong R F, et al. Fiber-optic two-way quantum time transfer with frequency-entangled pulses [J]. *Physical Review A*, 2019, 100(2): 023849.
- [5] Yabushita A, Kobayashi T. Spectroscopy by frequency-entangled photon pairs [J]. *Physical Review A*, 2004, 69(1): 013806.
- [6] Kalashnikov D A, Pan Z Y, Kuznetsov A I, et al. Quantum spectroscopy of plasmonic nanostructures [J]. *Physical Review X*, 2014, 4(1): 011049.
- [7] Stassi R, De Liberato S, Garziano L, et al. Spectral correlation measurements at the Hong-Ou-Mandel interference dip [J]. *Physical Review A*, 2015, 91(1): 013830.
- [8] Jin R B, Gerrits T, Fujiwara M, et al. Spectrally resolved Hong-Ou-Mandel interference between independent photon sources [J]. *Optics Express*, 2015, 23(22): 28836-28848.
- [9] Jin R B, Shimizu R. Extended Wiener-Khinchin theorem for quantum spectral analysis [J]. *Optica*, 2018, 5(2): 93-98.
- [10] Jin R B, Saito T, Shimizu R. Time-frequency duality of biphotons for quantum optical synthesis [J]. *Physical Review Applied*, 2018, 10(3): 034011.
- [11] Xiang X, Xiang X, Dong R F, et al. Hybrid frequency-time spectrograph for the spectral measurement of the two-photon state [J]. *Optics Letters*, 2020, 45(11): 2993-2996.
- [12] Dong S, Zhang W, Huang Y D, et al. Long-distance temporal quantum ghost imaging over optical fibers [J]. *Scientific Reports*, 2016, 6: 26022.
- [13] Yao X, Zhang W, Li H, et al. Long-distance thermal temporal ghost imaging over optical fibers [J]. *Optics Letters*, 2018, 43(4): 759-762.
- [14] Yao X, Liu X, You L X, et al. Quantum secure ghost imaging [J]. *Physical Review A*, 2018, 98(6): 063816.
- [15] Wu Z W, Qiu X D, Chen L X. Current status and prospect for correlated imaging technique [J]. *Laser & Optoelectronics Progress*, 2020, 57(6): 060001.
吴自文, 邱晓东, 陈理想. 关联成像技术研究现状及展望 [J]. *激光与光电子学进展*, 2020, 57(6): 060001.
- [16] Bennett C H, Brassard G, Crépeau C, et al. Teleporting an unknown quantum state via dual classical and Einstein-Podolsky-Rosen channels [J]. *Physical Review Letters*, 1993, 70(13): 1895.
- [17] Howell J C, Bennink R S, Bentley S J, et al. Realization of the Einstein-Podolsky-Rosen paradox using momentum- and position-entangled photons from spontaneous parametric down conversion [J]. *Physical Review Letters*, 2004, 92(21): 210403.
- [18] Xia, Y, Fu C B, Zhang S, et al. Probabilistic teleportation of an arbitrary three-particle state via a partial entangled four-particle state and a three-particle GHZ state [J]. *Journal of the Korean Physical Society*, 2005, 46(2): 388-392.
- [19] Deng F G, Long G L, Liu X S. Two-step quantum direct communication protocol using the Einstein-Podolsky-Rosen pair block [J]. *Physical Review A*, 2003, 68(4): 042317.
- [20] Zhu A D, Xia Y, Fan Q B, et al. Secure direct communication based on secret transmitting order of particles [J]. *Physical Review A*, 2006, 73(2):

- 022338.
- [21] Xia Y, Song H S. Controlled quantum secure direct communication using a non-symmetric quantum channel with quantum superdense coding[J]. *Physics Letters A*, 2007, 364(2): 117-122.
- [22] Hum D S, Fejer M M. Quasi-phasematching [J]. *Comptes Rendus Physique*, 2007, 8(2): 180-198.
- [23] Xu P, Zhu S N. Review article: quasi-phase-matching engineering of entangled photons[J]. *AIP Advances*, 2012, 2(4): 041401.
- [24] Jin R B, Chen G Q, Laudenbach F, et al. Thermal effects of the quantum states generated from the isomorphs of PPKTP crystal [J]. *Optics & Laser Technology*, 2019, 109: 222-226.
- [25] Kato K, Takaoka E. Sellmeier and thermo-optic dispersion formulas for KTP [J]. *Applied Optics*, 2002, 41(24): 5040-5044.
- [26] H C Photonics. PPLN guide: overview [EB/OL]. [2020-06-03]. <https://www.hcphotonics.com/ppln-guide-overview>.
- [27] Emanuelli S, Arie A. Temperature-dependent dispersion equations for KTiOPO_4 and KTiOAsO_4 [J]. *Applied Optics*, 2003, 42(33): 6661-6665.
- [28] Kalashnikov D A, Katamadze K G, Kulik S P. Controlling the spectrum of a two-photon field: inhomogeneous broadening due to a temperature gradient[J]. *JETP Letters*, 2009, 89(5): 224-228.
- [29] Jimenez G D, Garces V G, O'Donnell K A. Angular and temperature dependence of photon pair rates in spontaneous parametric down-conversion from a periodically poled crystal [J]. *Physical Review A*, 2017, 96(2): 023828.
- [30] Kakuno S, Fujimura M, Suhara T. Wavelength tuning by temperature control in MgO-doped LiNbO_3 waveguide quasi-phase-matching twin photon generation device [J]. *Japanese Journal of Applied Physics*, 2012, 51: 030201.
- [31] Kolev V Z, Duering M W, Luther-Davies B. Corrections to refractive index data of stoichiometric lithium tantalate in the 5-6 μm range [J]. *Optics Letters*, 2006, 31(13): 2033-2035.
- [32] Deng L H, Gao X M, Cao Z S, et al. Improvement to Sellmeier equation for periodically poled LiNbO_3 crystal using mid-infrared difference-frequency generation [J]. *Optics Communications*, 2006, 268(1): 110-114.
- [33] Zhang Y, Hou F Y, Liu T, et al. Generation and quantum characterization of miniaturized frequency entangled source in telecommunication band based on type-II periodically poled lithium niobate waveguide [J]. *Acta Physica Sinica*, 2018, 67(14): 144204. 张越, 侯飞雁, 刘涛, 等. 基于 II 类周期极化铌酸锂波导的通信波段小型化频率纠缠源产生及其量子特性测量 [J]. *物理学报*, 2018, 67(14): 144204.
- [34] Solli D R, Chou J, Jalali B. Amplified wavelength-time transformation for real-time spectroscopy [J]. *Nature Photonics*, 2008, 2(1): 48-51.
- [35] Chandrasekharan H K, Izdebski F, Gris-Sánchez I, et al. Multiplexed single-mode wavelength-to-time mapping of multimode light [J]. *Nature Communications*, 2017, 8: 14080.
- [36] Yang Y, Yang Y, Yang Y, et al. Inherent resolution limit on nonlocal wavelength-to-time mapping with entangled photon pairs [J]. *Optics Express*, 2020, 28(5): 7488-7497.
- [37] Wu J, You L, Chen S, et al. Improving the timing jitter of a superconducting nanowire single-photon detection system [J]. *Applied Optics*, 2017, 56(8): 2195-2200.
- [38] Grice W P, Walmsley I A. Spectral information and distinguishability in type-II down-conversion with a broadband pump [J]. *Physical Review A*, 1997, 56(2): 1627.
- [39] Fedrizzi A, Herbst T, Aspelmeyer M, et al. Antisymmetrization reveals hidden entanglement [J]. *New Journal of Physics*, 2009, 11(10): 103052.
- [40] Basiri-Esfahani S, Myers C R, Armin A, et al. Integrated quantum photonic sensor based on Hong-Ou-Mandel interference [J]. *Optics Express*, 2015, 23(12): 16008-16023.

Experimental Method for Fast Measuring the Phase-matched Wavelengths of Entangled Photons by Wavelength-to-Time Mapping

Li Baihong^{1,2}, Xia Zhiguang^{1,2}, Xiang Xiao^{2,3*}, Jin Yaqing^{2,3}, Quan Run'ai^{2,3},
Dong Ruifang^{2,3**}, Liu Tao^{2,3}, Zhang Shougang^{2,3}

¹ College of Sciences, Xi'an University of Science and Technology, Xi'an, Shaanxi 710054, China;

² Key Laboratory of Time and Frequency Primary Standards, National Time Service Center, Chinese Academy of Sciences, Xi'an, Shaanxi 710600, China;

³ School of Astronomy and Space Science, University of Chinese Academy of Sciences, Beijing 100049, China

Abstract

Objective The entangled photons generated by the spontaneous parameter down-conversion (SPDC) process have wide applications in quantum precision measurement, quantum spectroscopy, quantum imaging, quantum teleportation, and quantum security communications. However, one can only obtain a highly efficient SPDC when the phase-matching condition (conservation of momentum) is satisfied. In general, only a few birefringent crystals can meet the phase-matching condition, however the phase-matched wavelength (PMW) and bandwidth of entangled photons are limited. Afterwards, the quasi-phase matching (QPM) technology is proposed to solve the limitation problem of a birefringent crystal by artificially modulating the polling periods of the crystal. QPM is determined by the polling period and the refractive index of the crystal. The crystal temperature can be used to adjust the refractive index and different crystal temperatures are corresponding to different PMWs. To determine the crystal temperature at the required PMW, it is necessary to know the relationship between the PMW and crystal temperature. The temperature-dependent Sellmeier equation can be used to estimate this relationship. However, the Sellmeier equations of many nonlinear crystals are still unknown. Even if the Sellmeier equation is known, there is still a discrepancy between the estimated result and the experimental result in some special wavelengths and temperature ranges since the coefficients in the Sellmeier equation come from some empirical values. Thus, it needs to be revised or improved continuously. Therefore, it is necessary to use some experimental methods to accurately measure the PMW of the entangled photons in the SPDC process. In experiments, a monochromator is usually used to measure the spectrum of entangled photons and thus the relationship between the PMW and the crystal temperature is obtained. However, owing to the scanning for different wavelengths at different crystal temperatures, the measurement is low-accuracy and time-consuming, especially for the entangled broadband spectra.

Methods Herein, we propose an alternative experimental method for fast measuring the PMW of entangled photons versus crystal temperature. It utilizes the wavelength-to-time mapping (WTTM) technology with a dispersive element to realize a fast measurement. In the experimental setup (**Fig. 1**), the fiber Bragg grating is successively inserted in the signal and idler paths. By adjusting the crystal temperature, one can obtain the two curves of the time delay between arrival time of signal and idler photons versus crystal temperature. Further, based on the wavelength-to-time mapping relation, these two curves can be converted into those of the PMWs of the signal and idler photons versus the crystal temperature. Before the experiment, we first calibrate the WTTM relation by measuring the idler wavelength as a function of the time delay, in which the programmable filters and FBG are together input in the idler path. The utilized SPDC sources are generated from a 10 mm long, type-II periodically poled LiNbO₃ (PPLN, **Fig. 2**) waveguide and a periodically poled KTiOPO₄ (PPKTP, **Fig. 3**) crystal pumped by a continuous wave distributed Bragg reflector laser (DBR laser) at 780 nm. A half-wave plate is used to optimize the SPDC efficiency by adjusting the polarization of the pump laser. After filtering out the residual pump beam using two long-pass filters (LPPFs), the signal and idler photons are focused and then coupled into a fiber polarization beam splitter (FPBS). With the help of another half-wave plate, the signal and idler are separated into two polarization-orthogonal fiber paths marked using s and i, respectively. The coincidence count measurement is accomplished using a time-correlated single-photon counting module. According to our experimental results, we obtain a linear relation between the idler wavelength and the time delay, i. e., $\bar{\tau} = 893203 - 523.6l$. With this relation, we can estimate the FBG with $Dl = -(523.6 \pm 2.2) \text{ ps} \cdot \text{nm}^{-1}$ at 1560 nm.

Results and Discussions As examples, the experimental results are given with a PPLN waveguide (**Fig. 2**) and a PPKTP crystal (**Fig. 3**), which provides a proof for our proposed method. A measurement resolution better than 0.1 nm in **Fig. 2** is obtained owing to the use of two superconducting nanowire single-photon detectors (SNSPDs) with the maximum standard deviation of 47 ps from the five measurements of full-width half-maximum (FWHM) of $G^{(2)}$. A measurement resolution better than 0.27 nm in **Fig. 3** is obtained owing to the use of two semiconductor single-photon detectors with the maximum standard deviation of 143 ps using the same FBG. The measurement resolution in **Fig. 2** is better than that in **Fig. 3**, because the SNSPDs the former used can provide lower time jitters. The resolution is limited by the time jitters of the detectors and the magnitude of the dispersive elements. In principle, the smaller the jitter of the detector and the larger the amount of dispersion, the higher the resolution. Compared with the traditional method using a monochromator (a few hours), this method only takes a few minutes.

Conclusions In conclusion, we propose an alternative experimental method for fast measuring the PMW of entangled photons versus crystal temperature based on the WTTM technology. A measurement resolution better than 0.1 nm is obtained in our experiment and the measurement time is reduced significantly (only a few minutes) if compared with that of the traditional method using a monochromator (a few hours). In addition, we analyse the discrepancy between the theoretical and experimental results and discuss some possible applications. The proposed method can be applied to calibrate the poling period of crystals and the relation between PMW and crystal temperature, and is expected to modify or improve the temperature-dependent Sellmeier equations of nonlinear crystals.

Key words quantum optics; entangled photons; phase-matched wavelength; crystal temperature; wavelength-to-time mapping

OCIS codes 270.4180; 190.4410; 300.6320